



HAL
open science

Red-emitting tetraphenylethylene derivative with aggregation-induced enhanced emission for luminescent solar concentrators: A combined experimental and density functional theory study

Cosimo Micheletti, Qinfan Wang, Francesco Ventura, Michele Turelli, Ilaria Ciofini, Carlo Adamo, Andrea Pucci

► To cite this version:

Cosimo Micheletti, Qinfan Wang, Francesco Ventura, Michele Turelli, Ilaria Ciofini, et al.. Red-emitting tetraphenylethylene derivative with aggregation-induced enhanced emission for luminescent solar concentrators: A combined experimental and density functional theory study. *Aggregate*, 2022, 3 (2), pp.1501-1511. 10.1002/agt2.188 . hal-03855991

HAL Id: hal-03855991

<https://hal.science/hal-03855991>

Submitted on 16 Nov 2022

HAL is a multi-disciplinary open access archive for the deposit and dissemination of scientific research documents, whether they are published or not. The documents may come from teaching and research institutions in France or abroad, or from public or private research centers.

L'archive ouverte pluridisciplinaire **HAL**, est destinée au dépôt et à la diffusion de documents scientifiques de niveau recherche, publiés ou non, émanant des établissements d'enseignement et de recherche français ou étrangers, des laboratoires publics ou privés.

RESEARCH ARTICLE

Red-emitting tetraphenylethylene derivative with aggregation-induced enhanced emission for luminescent solar concentrators: A combined experimental and density functional theory study

Cosimo Micheletti¹ | Qinfan Wang² | Francesco Ventura¹ | Michele Turelli² |
 Ilaria Ciofini² | Carlo Adamo^{2,3} | Andrea Pucci¹ 

¹Department of Chemistry and Industrial Chemistry, University of Pisa, Pisa, Italy

²École nationale supérieure de chimie de Paris, Centre national de la recherche scientifique, Institute of Chemistry for Life and Health Sciences, PSL Research University, Paris, France

³Institut Universitaire de France, Paris, France

Correspondence

Carlo Adamo, Institute of Chemistry for Life and Health Sciences, Chimie ParisTech, 11, rue Pierre et Marie Curie, F-75005 Paris, France.

Email: carlo.adamo@chimieparistech.psl.eu

Andrea Pucci, Department of Chemistry and Industrial Chemistry, University of Pisa, Via Giuseppe Moruzzi 13, 56124 Pisa, Italy.

Email: andrea.pucci@unipi.it

Cosimo Micheletti and Qinfan Wang equally contributed to this work.

Funding information

MIUR-PRIN, Grant/Award Number:

20179BJNA2; European Union's Horizon 2020

Research and Innovation Program, Grant/Award

Number: 648558; China Scholarship Council,

Grant/Award Number: 202006890004

Abstract

This study examines the use of an aggregation-induced enhanced emission fluorophore (TPE-MR_h) to prepare red-emitting luminescent solar concentrators (LSCs) based on poly(methyl methacrylate) (PMMA) and poly(cyclohexyl methacrylate) (PCMA). TPE-MR_h is a tetraphenylethylene (TPE) derivative bearing two dimethylamino push groups and a 3-methyl-rhodanine pull moiety, with absorption maxima at around 500 nm and fluorescence peak at 700 nm that strongly increases in solid-state. TPE-MR_h displays a typical crystallization-induced enhanced emission that has been rationalized by modeling the compound behavior in solution and solid-state via density functional theory calculations with the inclusion of the environment. TPE-MR_h dispersed into 5 × 5 cm² polymer films with a thickness of 25 ± 5 μm has revealed a partial fluorescence quenching with fluorophore content. Quantum yields (QYs) below 10% for the 2 wt.% of doping have been addressed to the formation of less emissive micro-sized clusters of fluorophores. PMMA slabs with the same surface size but 3 mm of thickness and 200 ppm of TPE-MR_h have provided QY of 36.5% thanks to the attenuation of the detrimental effects of fluorophore aggregation. This feature is reflected in the LSCs performance, with devices achieving the largest power collected by the photovoltaic cell.

KEYWORDS

aggregation-induced enhanced emission, density functional theory, luminescent solar concentrators, poly(methyl methacrylate), tetraphenylethylene core

1 | INTRODUCTION

Nowadays, the most important techniques used to exploit solar energy consists of photovoltaic (PV) panels, but several other devices have been proposed over time.^[1,2] The thrust in PV keeps lowering the price per unit of power generated as the technology becomes more and more widespread. However, current PV panels are opaque and guarantee maximum performance under direct light conditions. Among the possible solutions, luminescent solar concentrators (LSCs) are one of the most promising approaches to further decrease the costs of PV and facilitate the integration of solar-harvesting devices into buildings. LSCs are slabs of a transparent

host material doped with high quantum yield (QY) fluorophores. The slab can be made entirely from plastic materials such as poly(methyl methacrylate) (PMMA) or polycarbonate or it can consist of a high purity optical glass coated with a thin film of the doped polymer. Incident sunlight is absorbed by the luminescent compounds in the slab and emitted at longer wavelengths. Thanks to the different refractive indexes of air and the dispersing matrix, fluorescence is then mostly concentrated, via total internal reflection, at the edges of the panel, where standard silicon solar cells are placed. Among the commonly used fluorophores are quantum dots, perovskites, rare-earth complexes, and organic molecules,^[3] possibly characterized by

This is an open access article under the terms of the [Creative Commons Attribution](https://creativecommons.org/licenses/by/4.0/) License, which permits use, distribution and reproduction in any medium, provided the original work is properly cited.

© 2022 The Authors. *Aggregate* published by SCUT, AIEI, and John Wiley & Sons Australia, Ltd.

large Stokes shifts (SS), and a suitable match between the emission wavelengths and the band-gap of the PV cells. The working mechanism of LSCs is affected by several adverse processes that decrease the efficiency with which light is delivered at the PV cells.^[4,5] For example, standard red-emitting organic fluorophores strongly quench their fluorescence in the condensed phase due to aggregation-caused quenching (ACQ). To overcome ACQ, the use of fluorophores characterized by aggregation-induced emission (AIE) or aggregation-induced enhanced emission (AIEE) has been recently proposed as an excellent alternative for photostable dopants in LSCs.^[6–8] Such fluorophores show weak emission in solution but display bright emission at high contents and in solid-state, an opposite behavior to ACQ.^[9,10] Among AIE/AIEE fluorophores, tetraphenylethylene (TPE) is the primary example.^[11] This molecule is characterized by a central olefin stator linked to four phenyl rotors. While these rotors can move freely in solvents with low viscosity, in solid-state, thanks to the restriction of intramolecular motions promoted by molecular packing, the same rotation is strongly constrained and the non-radiative relaxation associated is suppressed, yielding a bright solid-state fluorescence. Moreover, the TPE core can be easily functionalized with donor or acceptor functional groups^[7,12–21] to modulate the absorption and emission wavelengths and promote substantial SS that are beneficial to LSCs. Despite the use of TPE derivatives to better harness solar energy has already been proposed, the potential of AIE/AIEE materials to boost LSC performances is worth examining more closely. On this account, a new TPE derivative bearing two dimethylamino push groups and a 3-methyl-rhodanine pull moiety (**TPE-MRh**) was prepared. The fluorophore was characterized in terms of its AIE/AIEE behavior and to assess its potential use in LSCs. A thorough theoretical analysis supports the experimental data, offering a molecular-scale picture of the mechanisms underlying the observed behavior. Given the importance of the condensed-phase environment in the modulation of the photophysical properties involved,^[22] the modeling strategy employed combines the accurate simulation of the electronic structure of a single molecule with information on its local environment.^[23–25] The comparison between emissive properties in solution and aggregated phase allowed the rationalization of the AIE/AIEE character with molecular-level detail. LSC devices based on **TPE-MRh** were eventually prepared as thin-film and slab solar collectors to determine the differences between the two approaches in terms of the final performances.

2 | RESULTS AND DISCUSSION

2.1 | Synthesis of TPE-MRh

TPE-MRh fluorophore (Table 1) was prepared according to Scheme S1, that is, first through the assembly of the TPE core of the molecule by a McMurry reaction involving bis(dimethylamino) benzophenone and bromobenzophenone, in the presence of TiCl_4 and zinc powder.^[7] The obtained TPE derivative was then converted in the formylated product with dimethylformamide and eventually decorated with the 3-methyl-rhodanine by a typical Knoevenagel-type condensation.

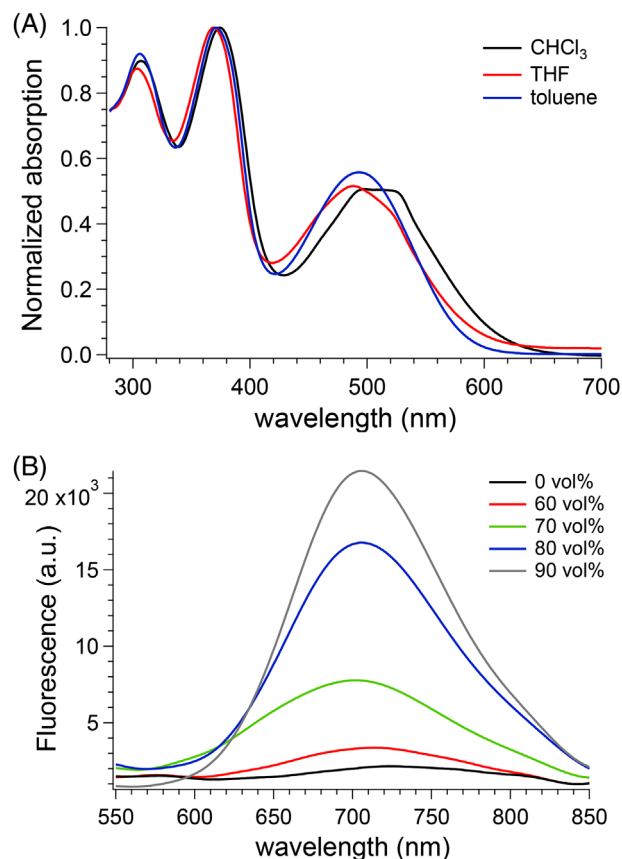


FIGURE 1 (A) Normalized absorption spectra of **TPE-MRh** in 5.0×10^{-5} M CHCl_3 , tetrahydrofuran (THF), and toluene solutions and (B) emission ($\lambda_{\text{exc}} 490$ nm) of **TPE-MRh** in 5.0×10^{-5} M of THF solution with different fractions of H_2O (vol%)

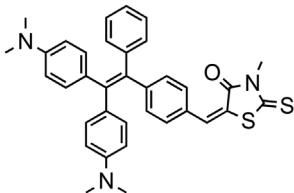
2.2 | Optical properties of TPE-MRh

The absorption and emission properties of **TPE-MRh** were determined in chloroform, toluene, and tetrahydrofuran (THF) solutions. **TPE-MRh** displays three absorption peaks at 303–307, 370–374, and 489–504 nm depending on the solvent (Figure 1A and Figures S6–S8), among them the middle peak is the most intense. For each solvent, different concentrations in the range of 10^{-6} – 10^{-5} M were analyzed, the absorption rises until it exceeds the unitary value for peaks at all wavelengths. Notably, in the range of concentrations of 10^{-6} – 10^{-3} M the emission intensity remains very low for all solvents (Figures S12–S14), although not completely suppressed.

The extinction molar coefficients (ϵ , Table 1), extrapolated from the linear fitting of the absorption data (Figures S9–S11), are maximum in THF (about $3.4 \times 10^4 \text{ M}^{-1} \text{ cm}^{-1}$), while the observed SS are well above 100 nm in all cases, and particularly prominent for THF and CHCl_3 , where SS values larger than 200 nm were recorded. These values are considered noteworthy and promising for the application of **TPE-MRh** in LSCs.

In order to determine the AIE/AIEE behavior of **TPE-MRh**, 5.0×10^{-5} M THF/water mixtures were examined. Notably, at water fractions larger than 60%–70%, **TPE-MRh** aggregates, thus boosting the fluorescence intensity with an emission peak at 705 nm (1.76 eV) (Figure 1B). The addition of water leads also to the formation of **TPE-MRh** nanoparticles, with an average diameter of 200 nm as confirmed

TABLE 1 Chemical structure of the **TPE-MRh** and the derived extinction molar coefficients and Stokes shifts (SS) of **TPE-MRh** in (A) CHCl_3 , (B) toluene, and (C) tetrahydrofuran (THF) solutions. In the case of CHCl_3 solution, the ϵ at the longest wavelength was not calculated because at lower concentrations (Figure S1) the signal consists of two different peaks that begin to coalesce to a unique broad peak at higher concentrations

TPE-MRh	CHCl_3	Toluene	THF
	$\epsilon_{307\text{nm}} = 23200 \text{ M}^{-1} \text{ cm}^{-1}$ $\epsilon_{374\text{nm}} = 25800 \text{ M}^{-1} \text{ cm}^{-1}$ SS = 233 nm	$\epsilon_{306\text{nm}} = 28600 \text{ M}^{-1} \text{ cm}^{-1}$ $\epsilon_{371\text{nm}} = 31000 \text{ M}^{-1} \text{ cm}^{-1}$ $\epsilon_{493\text{nm}} = 17600 \text{ M}^{-1} \text{ cm}^{-1}$ SS = 142 nm	$\epsilon_{304\text{nm}} = 29700 \text{ M}^{-1} \text{ cm}^{-1}$ $\epsilon_{369\text{nm}} = 33600 \text{ M}^{-1} \text{ cm}^{-1}$ $\epsilon_{489\text{nm}} = 17700 \text{ M}^{-1} \text{ cm}^{-1}$ SS = 218 nm

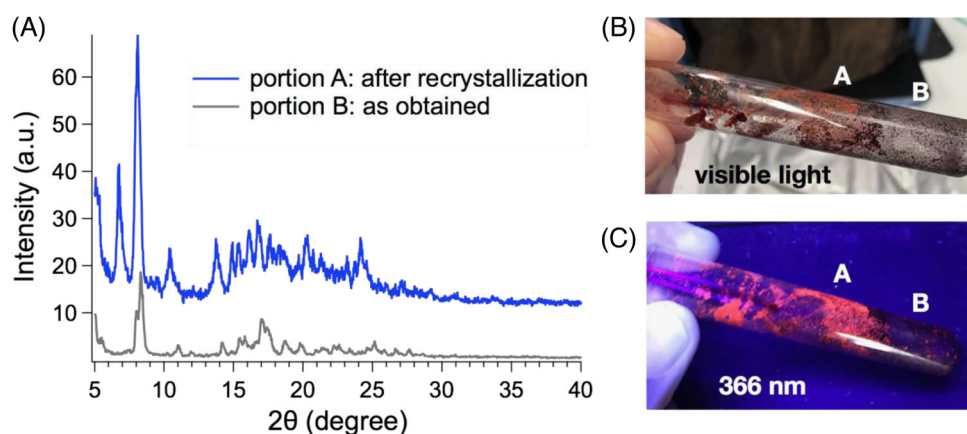


FIGURE 2 (A) X-ray diffraction (XRD) analysis of portion A (red crystalline) and portion B (dark amorphous) of **TPE-MRh** and photos of both portions of the **TPE-MRh** powder taken under (B) visible and (C) near UV light at 366 nm

by dynamic light scattering analysis (Figure S15). Despite the overall fluorescence magnification with the increasing amount of water, the faint but evident emission of **TPE-MRh** in pure THF suggested that the fluorophore could belong to the AIEE category instead of the AIE one.

It is worth noting that **TPE-MRh** has shown a solid-state polymorphic behavior. Indeed, a quick transition from solution to solid-phase led to poorly emissive dark amorphous solids. Conversely, after slow re-crystallization from THF/water mixtures, red-emissive crystal solids were obtained (Figure 2A,B). This phenomenon suggests that **TPE-MRh** displays a specific form of AIEE that may be better characterized as crystallization-induced enhanced emission (CIEE), as also evidenced by the X-ray diffractograms (XRDs) especially in the region at a low θ ($17\text{--}25^\circ$, Figure 2C). CIE and CIEE molecules^[26–29] are well known in literature and are characterized by a faint emission in solution and in an amorphous solid-state, while brighter fluorescence is displayed in the crystalline state.

2.3 | Theoretical modeling and analysis

In order to rationalize the observed optical behavior as a function of the solvent and aggregation state, a theoretical analysis of the **TPE-MRh** molecule has been performed in the two environments relevant to CIEE behavior, namely solution and crystalline phase. The details of the computational protocol adopted are reported in the Computational details section in the Supporting Information.

2.4 | Simulation in solution

Separate modeling has been considered for each of the solvents employed experimentally (see Figure S16). The absorption spectra in solution, simulated or measured, that are most relevant to our discussion are shown in Figure 3A. Blue and black curves indicate the simulated and measured absorption in THF. The energy of the vertical excitations calculated reproduces with reasonable accuracy the main experimental peaks.

A comparison between spectra simulated in the presence of an implicit solvent model for THF and water (blue and red lines) reveals that absorption is only slightly affected by the polarizability of the environment.

The low-energy peak can be attributed to the single electronic transition $S_0 \rightarrow S_1$. The calculated peak has a blueshift of 0.27 eV with respect to the experimental one, compatible with the typical accuracy of the method employed. The more pronounced difference in intensity instead, may be attributed to the presence of a vibrational contribution that is to be expected for a material displaying AIE/AIEE. The same transition is characterized by an intramolecular charge transfer from the two dimethylamino-decorated groups (labels A1 and A2 in Figure 3B) and the central ethylene core to the rhodanine-decorated (label Rh in Figure 3B) moiety. The magnitude of this transfer has been assessed through the use of the D_{CT} index^[30] that evaluates the electron-hole separation at the excited state. A rough comparison of the obtained value of 5.44 Å with the length of the longest molecular axis, 16.02 Å, defined by the central core, the A2 donor, and Rh

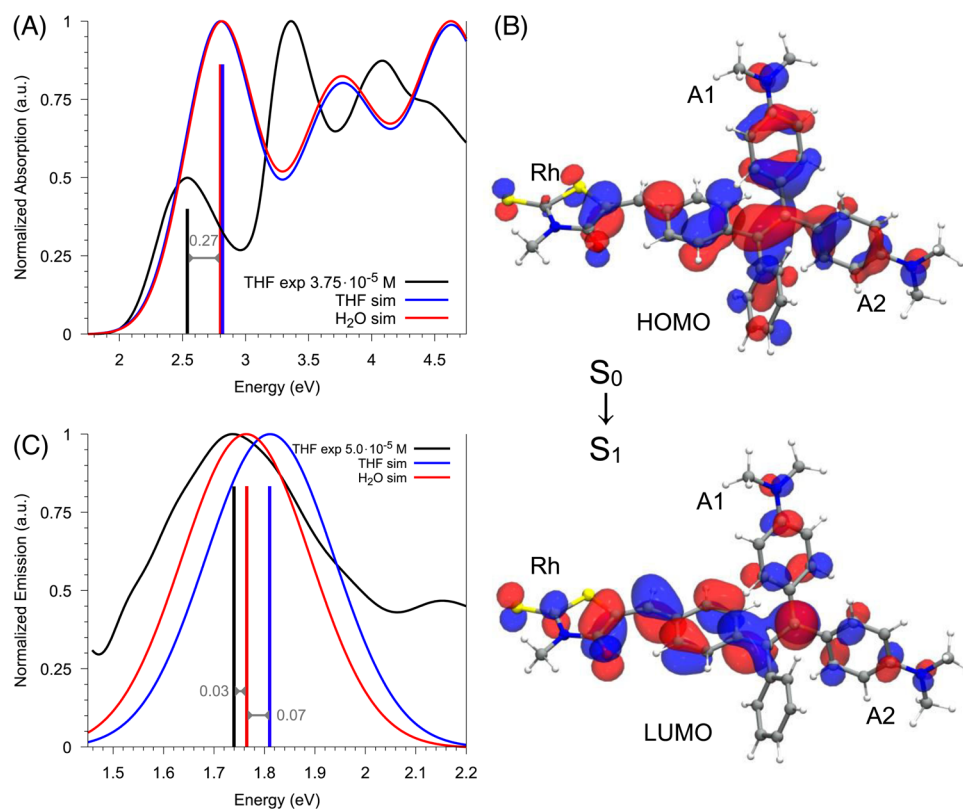


FIGURE 3 (A) Simulated UV-vis absorption spectra (FWHM = 0.66 eV) in tetrahydrofuran (THF) (blue) and water (red) and experimental UV-vis absorption spectrum in THF (black); (B) molecular orbitals mainly involved in the first transition $S_0 \rightarrow S_1$ (isodensity = 0.025 a.u.). **A1**, **A2** labels indicate the phenyls functionalized with the dimethylamino push groups while **Rh** refers to the phenyl functionalized with the rhodanine pull group; (C) simulated and experimental normalized emission spectrum of **TPE-MRh** in THF and water (FWHM = 0.26 eV)

acceptor, suggests a moderate intramolecular charge-transfer character, although it has to be considered that the computed value also weighs the electronic density transferred from the **A1** group. The $S_0 \rightarrow S_1$ transition mainly involves the highest occupied molecular orbital and lowest unoccupied molecular orbital. The first is distributed over the whole molecule while the second shows pronounced localization on **Rh**, as shown in Figure 3B. The transition energy can thus be modulated by changes in molecular geometry that determine a different coupling of the acceptor and donor moieties, particularly along the main axis.

In order to analyze the emissive properties of the **TPE-MRh** compound, the S_1 state has been relaxed. A comparison between the S_0 and S_1 relaxed structures indicates a planarization of the **Rh** moiety accompanied by a torsion of the **A2** moiety that becomes almost orthogonal to the approximate **Rh** moiety plane. Figure 3C reports the comparison between the experimental fluorescence in pure THF (black) and the simulated spectrum in the same solvent (blue). The $S_1 \rightarrow S_0$ emission energy is accurately reproduced at the level of theory employed (blueshifts of 0.03 and 0.07 eV for water and THF, respectively) but a discrepancy emerges: the predicted intense emission (with oscillator strength of 1.34) would indicate a large fluorescence QY in pure THF in clear disagreement with observations, see Figure 1B, black line.

This discrepancy is due to the existence of efficient non-radiative decay channels mediated by the vibrational degrees of freedom of the molecule that dominate the de-excitation process. The mechanism underlying these non-radiative channels cannot be captured by the theoretical framework adopted. However, it is possible to indirectly

assess their importance through the analysis of Huang-Rhys (HR) factors.^[31]

These factors are obtained by comparing relaxed molecular geometries and normal modes at the ground and excited states. Larger HR factors imply higher efficiencies of the non-radiative channels associated with molecular vibrations.

In order to facilitate the analysis, we compare the HR factors of **TPE-MRh** to those of the native TPE.^[11] TPE is an ideal reference because it displays complete suppression of fluorescence in solution while showing a pronounced solid-state emission characterized by considerable SS.^[6]

This comparison offers valuable insights into the mechanisms at play and also explains why **TPE-MRh** expresses a less pronounced AIE character that is better described as AIEE. The plot of the HR factors is reported in Figure S17.

With respect to TPE, which presents a set of large HR factors (the largest ones being 86.6 for the normal mode with 29.12 cm^{-1} and 51.95 for 260.40 cm^{-1}), **TPE-MRh** has its two largest HR factors in the low-frequency range with values much lower than TPE. The associated normal modes describe motions of the entire molecular structure that may indeed promote non-radiative decay.

More in detail, the mode boasting the largest factor (10.28 cm^{-1} , 38.06) is associated with a vibrating motion of the **Rh** pull moiety, sketched in Figure 4C. The same **Rh** moiety participates to the second largest factor (18.18 cm^{-1} , 13.78) that implies a vibration of the whole structure characterized in particular by a torsion of the rhodanine ring around the direction of its bond to the larger structure. The values of the HR factors and the associated motions reveal that **TPE-MRh** normal modes are substantially less coupled and its

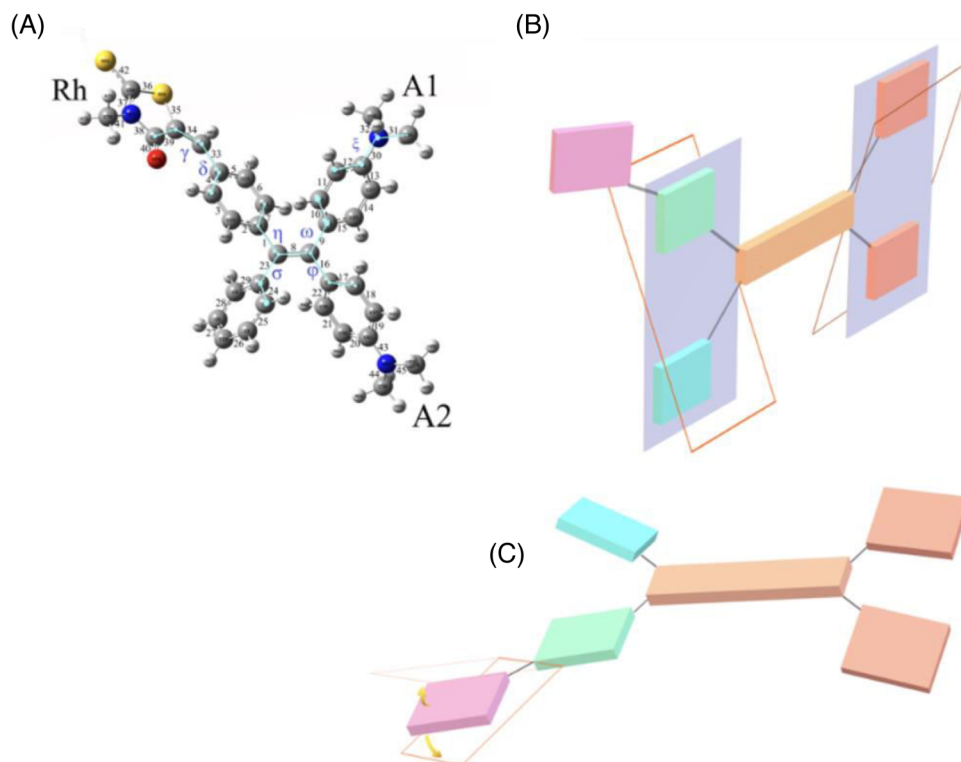


FIGURE 4 (A) Representation of the molecule with numbered bonds and relevant dihedrals of the molecule; (B) and (C) the rotation movement patterns of the molecule in the excitation

molecular structure experiences upon excitation a less pronounced structural reorganization that is not able to activate the non-radiative channels as much as in the case of unsubstituted TPE.

This observation supports the idea that the presence of non-radiative decay pathways is important in **TPE-MRh** and is responsible for its faint fluorescence but, contrary to TPE, the non-radiative decay is not able to completely suppress emission in solution due to the structural modifications brought forth by the grafting of the donor and acceptor groups.

In summary, the modeling of emission in solution reveals the existence of efficient non-radiative channels suppressing fluorescence in this phase that is responsible for the small observed QY.

2.5 | Simulation in the crystalline phase

As already remarked, experimental data indicate that aggregation mainly proceeds via the formation of small ordered aggregates, as suggested by the XRD patterns shown in Figure 2.

A likely CIEE behavior is signaled by the absence of broad peaks and the permanence of similar peaks upon recrystallization (Figure 2A, blue line) that justify our focus on fluorescent emission in a crystalline environment.

This environment has been simulated by considering the molecular packing obtained for a set of low-energy polymorphs identified via a sampling of **TPE-MRh** polymorph space. The selection of the final polymorph set has taken into account the agreement of each polymorph simulated XRD pattern to the experimental one and the computed thermodynamic stability ranking.

TABLE 2 The emission energies, wavelengths, and oscillator strengths of TPE-MRh polymorphs

Ranking	Space group	ΔE_{S1-S0} (eV)	λ (nm)	f
polymorph 1	Pna2 ₁	1.80	688.8	0.83
polymorph 2	P2 ₁ 2 ₁ 2 ₁	2.16	574.1	0.51
polymorph 3	P2 ₁ 2 ₁ 2 ₁	1.99	620.9	0.95
polymorph 4	Pna2 ₁	1.94	639.8	0.80

The set considered consists of four distinct polymorphs. Detailed data on these structures are reported in Table S1.

Through the application of an embedding procedure (see computational details of the Supporting Information) solid-state fluorescence has been computed for each polymorph.

Relevant observables are reported in Table 2. The comparison reveals that emission energy does not show any substantial change for the different crystal phases. Values are blueshifted in a range between +0.04 to +0.44 eV with respect to the experimental value of 1.76 eV, corresponding to the 705 nm peak reported in Figure 1B. The smallest blueshift is given by the lowest energy structure, polymorph 1, which maintains a relatively large oscillator strength of 0.83, see Figure 5A. This is consistent with the fluorescence displayed in the mixture of THF and water at 90% volume (Figure 1B, black line), where the addition of water has been shown to promote the formation of ordered aggregates to which emission can be ascribed.

Thus, the molecular system appears to maintain the same fluorescence energy when both diluted in a good solvent like THF and in the crystalline aggregates but experiences a considerable gain in brightness in the latter (roughly 6.7 more emissive in solid-state).

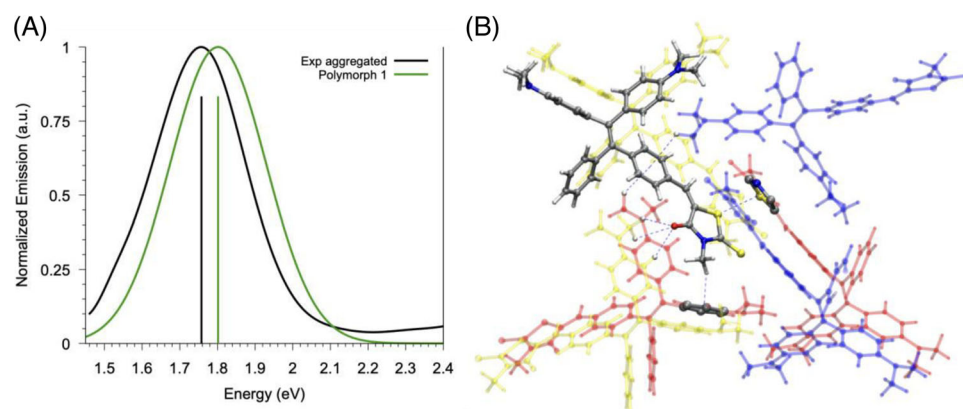


FIGURE 5 (A) Simulated emission spectrum of **TPE-MRh** polymorph 1 (FWHM = 0.30 eV) against experimental emission; (B) packing structure and the intermolecular distances of **TPE-MRh** polymorph 1

TABLE 3 Interaction distances in **TPE-MRh** polymorph 1

Interaction	Distance (Å)
A1 C-H... π Rh	3.1
A2 C-H... π Rh	2.9
A2 π ...H-C Rh	2.3
Rh π ...S Rh	3.2
A1 C-H...O Rh	2.6-2.7-3.0

This is compatible with the loss of efficiency for non-radiative de-excitation channels caused by the intermolecular interactions fostered by the crystalline packings. To better understand this, we have analyzed intermolecular distances in the four crystalline structures with particular focus on the constraints in place for the Rh moiety, identified in the previous HR study in solution as the responsible for the largest modulation effect. Within the two Pna₂1 packings, polymorphs 1 and 4, multiple intermolecular interactions can be identified. The C-H... π interactions mainly involve methyl-phenyl contacts of the Rh phenyl with methyl groups from A1 and A2. While the methyl of the Rh group interacts with the phenyl of another close A2 group. In addition, the O and S atoms in the Rh heterocycle retain localized lone pairs that favor interactions of the type C-H...O with multiple C-H belonging to an A1 moiety or of type π ...S involving Rh groups of neighboring molecules. The interactions are sketched in Figure 5B. These interactions may strongly hamper Rh group vibrations, hence suppressing the non-radiative channels associated with them and making the radiative process dominant. For the other two polymorphs, similar π ...S and C-H... π interactions are equally present and equivalent constraints are in place. Distances between the relevant groups identified are reported in Table 3.

These interactions seem to play a major role in generating structural constraints that effectively hamper the vibrations associated with non-radiative decay and result in the conspicuous enhancement of solid-state fluorescence. This is further demonstrated by the analysis of how a few relevant dihedrals, indicated in Figure 4 and Figure S18, vary between S₀ and S₁ relaxed geometries in solution and the crystal polymorphs. The corresponding values are given in Table S2. The comparison reveals that the four dihedrals quantifying the torsion of the moieties linked to the central stator (η , ω , ν , and

λ) experience, during excited-state reorganization in crystal phase, sensibly smaller variations than the ones predicted in solution, again proving the constraining effect of the crystalline phase. The two motions mostly concerned are the rotations of phenyls of the Rh and A1 moieties and the rotation between the two sets of geminal groups around the central stator.

The role of the tight crystalline packing appears therefore central to **TPE-MRh** CIEE behavior. This is compatible with reported data indicating that the amorphous packing, displaying less structured intermolecular interactions, is not sufficient to achieve fluorescence enhancement.

2.6 | Preparation and characterization of LSC based on **TPE-MRh**

Before the final application of **TPE-MRh** as a dopant in LSC, TGA analysis determined the thermal stability of the fluorophore. Notably, **TPE-MRh** revealed good stability under the processing and working conditions in solar plastic collectors since the main weight loss occurred at a temperature higher than 300°C (Figure S19).

TPE-MRh was then dispersed in transparent and totally amorphous PMMA and poly(cyclohexyl methacrylate) (PCMA) matrices at different concentrations (0.4–2.0 wt.%). Thin-film LSCs were realized by drop-casting of **TPE-MRh**/PMMA and **TPE-MRh**/PCMA chloroform solution on high-optical purity 5 × 5 × 0.3 cm³ glasses. The thickness of 25 ± 5 μm was obtained after solvent evaporation.

In PMMA and PCMA films, **TPE-MRh** exhibited the typical absorption bands in the 300–500 nm interval (Figure 6A), with intensity, regularly increasing with concentration (Figure 6B) and without evident differences in the spectral shape with respect to those in solution (Figures S9–S11). In addition, no evident absorption bands attributed to aggregates in polymer films were observed. In agreement with the RIM mechanism that occurred in a highly viscous solid matrix, **TPE-MRh** displayed a fluorescence band that encompasses the 500–800 nm spectral range (Figure 10), without evident vibronic contributions even at high doping. The shape of the emission band remained unaltered at different fluorophore concentrations but showed a progressive red-shift, possibly caused by auto-absorption phenomena (i.e., inner filter effects).^[32] Notably, SS of more than

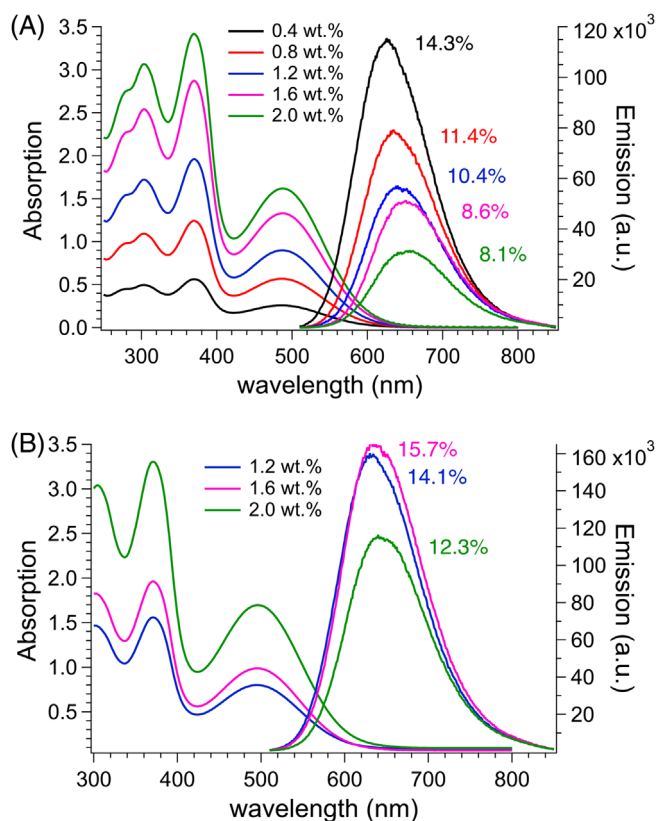


FIGURE 6 Absorption and emission spectra (λ_{exc} 490 nm) of **TPE-MRh** dispersed at different concentrations (0.4–2.0 wt.%) in (A) poly(methyl methacrylate) (PMMA) and (B) poly(cyclohexyl methacrylate) (PCMA) thin films. The data near the fluorescence bands are the respective quantum yield (QY, %)

130 nm were observed for both **TPE-MRh**/PMMA and **TPE-MRh**/PCMA films at the lowest fluorophore content. However, the maximum QY values recorded were around 14%–16% and progressively decreased with **TPE-MRh** concentration below 10% for PMMA films. This result was not surprising because similar TPE-based AIE fluorophores experienced in polymer films similar ACQ phenomena and the behavior was addressed to the formation of less emissive amorphous aggregates.^[6–8] This is in agreement with the CIEE characteristics of **TPE-MRh**, that is, the addition of progressive amounts of fluorophore in the highly viscous glassy polymer matrix did not favor the formation of well-packed ordered assemblies of the fluorophore. Notably, annealing procedures at 110°C, which is just above the glass transition temperature (T_g) of PMMA (105°C) did not provide any variation of the fluorescence intensity. In PCMA, fluorescence quenching with fluorophore content appeared less pronounced possibly

TABLE 4 TPE-MRh/PMMA thin film luminescent solar concentrator (LSC) performances. P_r values are characterized by relative errors of 0.01

TPE-MRh/PMMA LSC	QY (%)	P_r	
		Black matte layer	Diffusive layer
0.4 wt.%	14.3	1.15	1.55
0.8 wt.%	11.4	1.35	1.68
1.2 wt.%	10.4	1.30	1.66
1.6 wt.%	8.6	1.40	1.70
2.0 wt.%	8.1	1.31	1.59

Abbreviations: LSC, luminescent solar concentrator; PMMA, poly(methyl methacrylate); QY, quantum yield.

due to better phase compatibility between **TPE-MRh** and the polymer matrix, in agreement with recent results.^[32]

TPE-MRh visually showed a good dispersion in the polymer matrices (Figures S20 and S21), which appeared homogenous at a macroscopic level, and with negligible phase separation at the film surface even at the highest fluorophore content. Inspection of fluorescence microscopy images revealed the formation of microscopic emissive particles with a length of less than 25 μm on average. PCMA films showed better compatibility with respect to PCMA but cracks on the surfaces occurred just a few hours after the film formation (Figure 7).

This phenomenon was not attributed to the different T_g of PCMA (104°C, i.e., practically identical to PMMA) but to the lower polarity of the matrix^[32,33] that possibly interacts worse with the glass surface, thus causing film breaking. The lower polarity of PCMA with respect to PMMA was confirmed by water contact angle measurements. Note that, 72° for the former and 60° for the latter were indeed measured. Therefore, **TPE-MRh**/PCMA films were then discarded for successive investigations.

Polymer thin films LSC with a thickness of $25 \pm 5 \mu\text{m}$ and containing **TPE-MRh** at different concentrations (0.4–2.0 wt.%) were prepared by drop-casting on a $50 \times 50 \times 3 \text{ mm}^3$ optically pure glass substrate with polished surfaces. The LSC was connected to a Si-based PV cell (see Supporting Information for details) that was masked with black tape to match the LSC edge so that limiting the stray light to negligible levels. Silicon was used to grease the LSC edge. The other three edges of the LSC were covered with reflective aluminum tape. The LSC performances were evaluated by calculating the ratio (P_r) between the power generated by the LSC connected to a PV cell (P_{LSC}) and the power of the PV cell (P_{PV}) directly exposed to the illumination of an AM1.5G solar simulator under one sun (Table 4). We are aware that

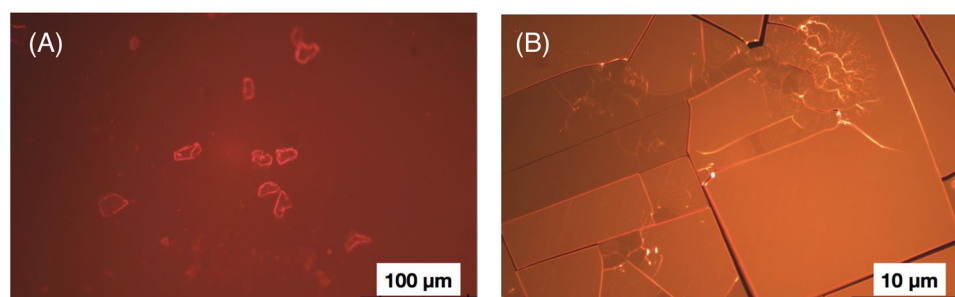


FIGURE 7 Fluorescent microscopy images of (A) 2 wt.% **TPE-MRh**/PMMA and (B) 2 wt.% **TPE-MRh**/PCMA films

this procedure did not perfectly match with the protocols recently published in the specialized literature^[34–36] but it was anyway useful to determine the influence of the **TPE-MRh** contents and LSC architecture on the overall device performances. Notably, P_r was determined also by using a white diffusive backscattering layer beneath the LSC slab (about 2.5 mm gap) with the aim to determine the influence of the backscattered radiation.

All **TPE-MRh**/PMMA LSCs showed P_r higher than 1, thus suggesting that all the prepared LSCs were able to effectively concentrate the emitted fluorescence on the PV cell. Notably, growing P_r values with fluorophore content were attributed to the solar harvesting characteristics of **TPE-MRh** that were maximized at 1.6 wt.%. The presence of the scattering diffusive layer boosted the power ratio as analogously reported in the literature.^[37,38] Conversely, P_r dropped consistently to 1.31 and 1.59 at the highest content, possibly due to fluorescence quenching caused by the formation of unemissive **TPE-MRh** supramolecular structures and in agreement with the lowest value of QY (8.1%).

With the aim of gathering the maximum solar harvesting without compromising the concentration efficiency of the fluorescence emitted by the LSC, a change in the LSC preparation was proposed. Ideally, an LSC PMMA slab with the same thickness of 3 mm as the corresponding LSC made by glass covered by the active thin film of about 30 μm , allowed to decrease the **TPE-MRh** concentration of about 100. A lower amount of fluorophore able to provide the same solar harvesting features possibly allows us to decrease the detrimental effects caused by the formation of an excessive amount of interacting **TPE-MRh** fluorophores. A $5 \times 5 \times 0.3 \text{ cm}^3$ LSC PMMA slab with polished surfaces containing 200 ppm of **TPE-MRh** was therefore fabricated via in-situ cell casting polymerization of MMA^[39] and the results compared with the corresponding thin-film architecture containing the 2 wt.% of the fluorophore.

TPE-MRh in the LSC slab showed the same optical absorption bands peaked at 360 and 470 nm and fluorescence maximum at about 630 nm, that is, both slightly blue-shifted of a few nm with respect to the thin film LSC (Figure 8A). It is worth noting that the QY of 36.5% measured for the LSC slab containing 200 ppm of fluorophore that was the highest ever registered for **TPE-MRh**. Moreover, the fluorescence microscopy image (Figure 8B) displayed a highly homogeneous distribution of the fluorophore within the PMMA slab and without the presence of microscopic aggregates as revealed in the PMMA thin film in Figure 7A. These results were also flanked by the 1.42 and 1.78 values of P_r calculated by using a black matte and scattering layers, respectively, the highest power ratio provided by the LSC prepared in this work starting from **TPE-MRh**. P_r was also calculated starting from a PMMA slab of the same size but devoid of any amount of **TPE-MRh** with the aim to determine the influence of the stray light. Values of 0.6–0.7 were gathered under identical illumination conditions and with the use of the diffusive scattering layer. By placing a black matte layer, P_r decreased to 0.3.

Overall, these worthwhile results confirmed that the LSC PMMA slab is the ideal solution to boost the concentration efficiencies of solar collectors based on fluorophores that suffer from the detrimental effects due to fluorophore aggregation. Also in the case of AIE and AIEE fluorophores, the slab

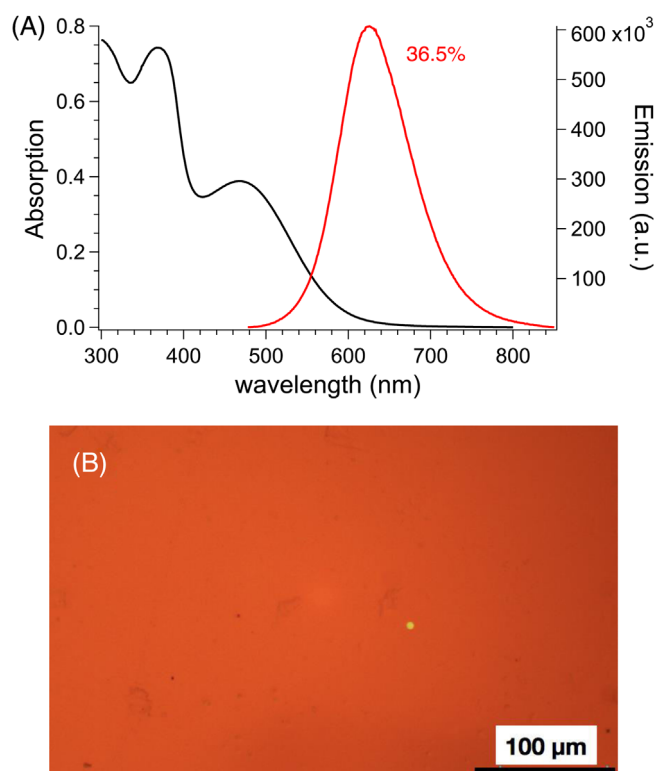


FIGURE 8 (A) Absorption and emission spectra (λ_{exc} 490 nm) of poly(methyl methacrylate) luminescent solar concentrator (PMMA LSC) slab containing 200 ppm of **TPE-MRh**. The data near the fluorescence band is the respective quantum yield (QY, %); (B) fluorescent microscopy image of the same LSC

solution should be preferred to the thin film one if the formation of amorphous aggregates is accompanied by fluorescence quenching.

3 | CONCLUSIONS

We have synthesized a new thermally-stable red-emitting AIEE fluorophore, that is, **TPE-MRh**, based on the TPE core and decorated with dimethylamino donor and 3-methylrhodanine pull groups. **TPE-MRh** shows maximum absorptions around 500 nm and a faint fluorescence at about 700 nm in solution, which displays a strong enhancement upon the addition of water that induces aggregation. The theoretical investigation has allowed elucidating the mechanism responsible for this fluorescence enhancement by proving how non-radiative decay channels associated with molecular vibrations lose efficiency going from solution to the crystalline phase. This confirms the AIEE character of the compound that can be characterized more precisely as CIEE. A set of crystal packings with the largest probability of being represented at experimental conditions have been proven to provide similar constraints to the molecular vibrations identified as the largest contributors to non-radiative de-excitation in solution. **TPE-MRh** incorporated into PMMA and PCMA films with $25 \pm 5 \mu\text{m}$ of thickness at concentrations of 0.4–2 wt.% revealed a homogeneous phase dispersion at a macroscopic level with the formation of a few microscopic fluorophore aggregates of less than 25 μm length at the highest content. Films based on PCMA experienced cracks formation on the surface just a few hours after the film formation, possibly due to the lower

polarity than PMMA that limits the effective interaction with the glass surface.

All the $5 \times 5 \text{ cm}^2$ thin-film LSCs showed P_r higher than 1, thus confirming their ability to concentrate the emitted fluorescence on the PV cell, but the performances were adversely affected by the **TPE-MR_h** content due to the progressive quenching of the fluorescence caused by the formation of less emissive amorphous aggregates. Note that, $5 \times 5 \text{ cm}^2$ LSCs based on PMMA slab with 3 mm of thickness and 200 ppm of **TPE-MR_h** displayed the highest QY of 36.5% and maximum P_r of 1.78. This result supports the idea to limit the detrimental effects caused by aggregation also in the case of AIE and AIEE molecules by incorporating fluorophore molecules in thick plastic slabs instead of polymer thin films deposited on glass.

4 | EXPERIMENTAL SECTION

TPE-MR_h was prepared in agreement with literature reports.^[7,13,40] LSCs based on polymeric films containing **TPE-MR_h** were obtained with a thickness of $25 \pm 5 \mu\text{m}$ and following a procedure reported in the literature.^[41] LSC based on PMMA slab containing **TPE-MR_h** was obtained with a thickness of 3 cm and following a method already published.^[42,43] LSCs were characterized in agreement with a procedure already reported by the same group. All the experimental details and computational procedures were detailed reported in the Supporting Information section.

ACKNOWLEDGMENTS

This work was supported by the MIUR-PRIN 20179BJNA2. This project has also received funding from the European Research Council (ERC) under the European Union's Horizon 2020 Research and Innovation Program (grant agreement no. 648558 STRIGES CoG). Support from grant no. H2020-MSCA-ITN-2017 training network "COSINE-Computational Spectroscopy In Natural sciences and Engineering" is also acknowledged. Q.W. acknowledges the financial support from the China Scholarship Council (grant no. 202006890004).

CONFLICT OF INTEREST

The authors declare no competing interests.

DATA AVAILABILITY STATEMENT

The data that support the findings of this study are available from the corresponding author upon reasonable request.

ORCID

Andrea Pucci  <https://orcid.org/0000-0003-1278-5004>

REFERENCES

- G. H. Bauer, *Photovoltaic Solar Energy Conversion*, Springer Verlag GmbH Berlin, Heidelberg **2015**.
- N. Armadori, V. Balzani, *Chem. A Eur. J.* **2016**, *22*, 32.
- J. Roncali, *Adv. Energy Mater.* **2020**, *10*, 2001907.
- C. Tummelshammer, A. Taylor, A. J. Kenyon, I. Papakonstantinou, *Sol. Energy Mater. Sol. Cells* **2016**, *144*, 40.
- M. G. Debije, P. P. C. C. Verbunt, *Adv. Energy Mater.* **2012**, *2*, 12.
- F. De Nisi, R. Francischello, A. Battisti, A. Panniello, E. Fanizza, M. Striccoli, X. Gu, N. L. C. Leung, B. Z. Tang, A. Pucci, *Mater. Chem. Front.* **2017**, *1*, 1406.
- R. Mori, G. Iasilli, M. Lessi, A. B. Muñoz-García, M. Pavone, F. Bellina, A. Pucci, *Polym. Chem.* **2018**, *9*, 1168.
- A. Pucci, *Isr. J. Chem.* **2018**, *58*, 837.
- Y. Hong, J. W. Y. Lam, B. Z. Tang, *Chem. Soc. Rev.* **2011**, *40*, 5361.
- J. Mei, N. L. C. Leung, R. T. K. Kwok, J. W. Y. Lam, B. Z. Tang, *Chem. Rev.* **2015**, *115*, 11718.
- G. Iasilli, A. Battisti, F. Tantussi, F. Fuso, M. Allegrini, G. Ruggeri, A. Pucci, *Macromol. Chem. Phys.* **2014**, *215*, 499.
- X. Wang, Z. Zhao, T. Xue, Z. Tan, Z. Song, S. Wei, Y. Bo, Y. Wang, J. Cheng, *Prog. Nat. Sci. Mater. Int.* **2021**, *31*, 541.
- E. Wang, E. Zhao, Y. Hong, J. W. Y. Y. Lam, B. Z. Tang, *J. Mater. Chem. B* **2014**, *2*, 2013.
- J. Xiong, K. Wang, Z. Yao, B. Zou, J. Xu, X.-H. H. Bu, *ACS Appl. Mater. Interfaces* **2018**, *10*, 5819.
- A. Chatterjee, D. G. Khandare, P. Saini, A. Chattopadhyay, M. S. Majik, M. Banerjee, *RSC Adv.* **2015**, *5*, 31479.
- W. Qin, K. Li, G. Feng, M. Li, Z. Yang, B. Liu, B. Z. Tang, *Adv. Funct. Mater.* **2014**, *24*, 635.
- Z. Chang, Y. Jiang, B. He, J. Chen, Z. Yang, P. Lu, H. S. Kwok, Z. Zhao, H. Qiu, B. Z. Tang, *Chem. Commun.* **2012**, *49*, 594.
- N. Zhao, M. Li, Y. Yan, J. W. Y. Y. Lam, Y. L. Zhang, Y. S. Zhao, K. S. Wong, B. Z. Tang, K. S. Wong, B. Z. Tang, *J. Mater. Chem. C* **2013**, *1*, 4640.
- Z. Zhao, C. Y. K. K. Chan, S. Chen, C. Deng, J. W. Y. Y. Lam, C. K. W. W. Jim, Y. Hong, P. Lu, Z. Chang, X. Chen, H. S. Kwok, H. Qiu, B. Z. Tang, P. Lu, H. S. Kwok, H. Qiu, B. Z. Tang, *J. Mater. Chem.* **2012**, *22*, 4527.
- M. T. Gabr, F. C. Pigge, *RSC Adv.* **2015**, *5*, 90226.
- X. Chen, X. Y. Shen, E. Guan, Y. Liu, A. Qin, J. Z. Sun, B. Zhong Tang, *Chem. Commun.* **2013**, *49*, 1503.
- Y. Hong, J. W. Y. Lam, B. Z. Tang, *Chem. Commun.* **2009**, *29*, 4332.
- D. Presti, L. Wilbraham, C. Targa, F. Labat, A. Pedone, M. C. Menziani, I. Ciofini, C. Adamo, *J. Phys. Chem. C* **2017**, *121*, 5747.
- L. Wilbraham, M. Louis, D. Alberga, A. Brosseau, R. Guillot, F. Ito, F. Labat, R. Métivier, C. Allain, I. Ciofini, *Adv. Mater.* **2018**, *30*, 1800817.
- L. Le Bras, C. Adamo, A. Perrier, *J. Phys. Chem. C* **2017**, *121*, 25603.
- Y. Dong, J. W. Y. Y. Lam, A. Qin, Z. Li, J. Sun, H. H. Y. H.-Y. Sung, I. D. Williams, B. Z. Tang, *Chem. Commun.* **2006**, *1*, 40.
- S. Ohtani, M. Gon, K. Tanaka, Y. Chujo, *Chemistry* **2017**, *23*, 11827.
- Y. Dong, J. W. Y. Y. Lam, A. Qin, J. J. Sun, J. Liu, Z. Li, J. J. Sun, H. H. Y. Y. Sung, I. D. Williams, H. S. Kwok, B. Z. Tang, *Chem. Commun.* **2007**, *31*, 3255.
- C. Zheng, Q. Zang, H. Nie, W. Huang, Z. Zhao, A. Qin, R. Hu, B. Z. Tang, *Mater. Chem. Front.* **2017**, *2*, 180.
- T. Le Bahers, C. Adamo, I. Ciofini, *J. Chem. Theory Comput.* **2011**, *7*, 2498.
- K. Huang, A. Rhys, *Selected Papers of Kun Huang*, World Scientific, Singapore **2000**.
- C. Papucci, R. Charaf, C. Coppola, A. Sinicropi, A. Mariangela, D. Donato, M. Taddei, P. Foggi, A. Battisti, B. De Jong, L. Zani, A. Mordini, A. Pucci, M. Calamante, G. Reginato, *J. Mater. Chem. C* **2021**, *9*, 15608.
- F. J. Ostos, G. Iasilli, M. Carloti, A. Pucci, *Polymers* **2020**, *12*, 2898.
- M. G. Debije, R. C. Evans, G. Griffini, *Energy Environ. Sci.* **2021**, *14*, 293.
- C. Yang, D. Liu, R. R. Lunt, *Joule* **2019**, *3*, 2871.
- C. Yang, H. A. Atwater, M. A. Baldo, D. Baran, C. J. Barile, M. C. Barr, M. Bates, M. G. Bawendi, M. R. Bergren, B. Borhan, C. J. Brabec, S. Brovelli, V. Bulović, P. Ceroni, M. G. Debije, J.-M. Delgado-Sanchez, W.-J. Dong, P. M. Duxbury, R. C. Evans, S. R. Forrest, D. R. Gamelin, N. C. Giebink, X. Gong, G. Griffini, F. Guo, C. K. Herrera, A. W. Y. Ho-Baillie, R. J. Holmes, S.-K. Hong, T. Kirchartz, B. G. Levine, H. Li, Y. Li, D. Liu, M. A. Loi, C. K. Luscombe, N. S. Makarov, F. Mateen, R. Mazzaro, H. McDaniel, M. D. McGehee, F. Meinardi, A. Menéndez-Velázquez, J. Min, D. B. Mitzi, M. Moemeni, J. H. Moon, A. Nattestad, M. K. Nazeeruddin, A. F. Nogueira, U. W. Paetzold, D. L. Patrick, A. Pucci, B. P. Rand, E. Reichmanis, B. S. Richards, J. Roncali, F. Rosei, T. W. Schmidt, F. So, C.-C. Tu, A. Vahdani, W. G. J. H. M. van Sark, R. Verduzco, A. Vomiero, W. W. H. Wong, K. Wu, H.-L. Yip, X. Zhang, H. Zhao, R. R. Lunt, *Joule* **2022**, *6*, 8.
- A. H. Zewai, J. S. Batchelder, T. Cole, *Appl. Opt.* **1979**, *18*, 3090.
- G. Iasilli, R. Francischello, P. Lova, S. Silvano, A. Surace, G. Pesce, M. Alloisio, M. Patrini, M. Shimizu, D. Comoretto, A. Pucci, *Mater. Chem. Front.* **2019**, *3*, 429.

39. S. Mattiello, A. Sanzone, F. Bruni, M. Gandini, V. Pinchetti, A. Monguzzi, I. Facchinetti, R. Ruffo, F. Meinardi, G. Mattioli, M. Sassi, S. Brovelli, L. Beverina, *Joule* **2020**, *4*, 1988.
40. M. Hauck, M. Stolte, J. Schönhaber, H.-G. G. Kuball, T. J. J. Müller, J. Schönhaber, H.-G. G. Kuball, T. J. J. Müller, *Chem. - A Eur. J.* **2011**, *17*, 9984.
41. M. Carlotti, G. Ruggeri, F. Bellina, A. Pucci, *J. Lumin.* **2016**, *171*, 215.
42. A. Sanguineti, M. Sassi, R. Turrise, R. Ruffo, G. Vaccaro, F. Meinardi, L. Beverina, *Chem. Commun.* **2013**, *49*, 1618.
43. F. Meinardi, A. Colombo, K. A. Velizhanin, R. Simonutti, M. Lorenzon, L. Beverina, R. Viswanatha, V. I. Klimov, S. Brovelli, *Nat. Photonics* **2014**, *8*, 392.

SUPPORTING INFORMATION

Additional supporting information may be found in the online version of the article at the publisher's website.

How to cite this article: C. Micheletti, Q. Wang, F. Ventura, M. Turelli, I. Ciofini, C. Adamo, A. Pucci, *Aggregate* **2022**, *3*, e188.
<https://doi.org/10.1002/agt2.188>